International Journal of Fluid Machinery and Systems
Vol. 2, No. 3, July-September 2009

Original Paper

Study for the Increase of Micro Regenerative Pump Head

Hironori Horiguchi [1], Keisuke Wakiya [1], Yoshinobu Tsujimoto [1], Masaaki Sakagami [2] and Shigeo Tanaka [2]

[1] Graduate School of Engineering Science, Osaka University
1-3 Machikaneyama, Toyonaka, Osaka, 560-8531, Japan
[2] Taisei Kogyo Co., Ltd.
26-1 Ikedakita, Neyagawa, Osaka, 572-0073, Japan

Abstract

The effect of inlet and outlet blade angles on a micro regenerative pump head was examined in experiments. The pump head was little increased by changing the blade angles compared with the original pump with the inlet and outlet blade angles of 0 degree. The effect of the axial clearance between the impeller and the casing on the pump head was also examined. The head was increased largely by decreasing the axial clearance. The computation of the internal flow was performed to clarify the cause of the increase of the pump head due to the decrease of the clearance. The local flow rate in the casing decreased as the leakage flow rate through the axial clearance decreased due to the decrease of the clearance. It was found that the larger head in the smaller clearance was just caused by the smaller local flow rate in the casing. In the case of the smaller clearance, the smaller local flow rate caused the smaller circumferential velocity near the front and rear sides of the impeller. This caused the increase of the angular momentum in the casing and the head.

Keywords: Micro Regenerative Pump, Internal Flow, Blade Angle, Clearance, Leakage Flow

1. Introduction

High pressure micro pumps with the impeller diameter of a few millimeters are expected for fuel supply to fuel cells. The micro pump is also required in the fields of micro, bio, and chemical applications and energy-related devices such as micro heat exchangers. A regenerative pump has desirable characters of high discharge pressure and continuous discharge. Therefore, the development of a micro regenerative pump with the impeller diameter of about 10mm has been carried out in our research group [1].

In the previous study, it was found that the pump head increased at low flow rates as the Reynolds number decreased [2] and the pump head increased by attaching vanes on both sides of the impeller due to the decrease of the leakage flow rate through the clearance between the impeller and the casing [3]. The pump head of the symmetric impeller with vanes on both sides was about 2.5 times as large as that of the asymmetric impeller with vanes on one side, but the pump head was about two third of our desired pump head.

In the present study, the increase of the pump head was attempted by adjusting the inlet and outlet blade angles and the decrease of the axial clearance between the impeller and the casing. These effects for the pump head were examined in experiments and computations using the commercial software, CFX-11.0.

2. Experimental Setup and Experiment

The schematic of the regenerative pump and the coordinate system are shown in Fig.1. Figure 2 shows the cross section of the test pump. The materials of the impeller and the casing are aluminum and transparent acrylic resin, respectively. The values of the parameters shown in Figs. 1 and 2 are given in Table 1. For the accurate adjustment of the clearance between the impeller and the casing, which would largely affect the performance, the size of the pump is increased to about ten times of the targeted micro regenerative pump. The diameter of the impeller D_T is 75mm and the axial clearance c_1 between the impeller and the casing in the original pump is 1.2mm. The thickness of the vane is 5 mm so that it is not extremely thin in real micro regenerative pump. The larger clearance and the larger thickness of the vanes are different from conventional regenerative pumps. The clearance c_1 is changed into 0.6mm by attaching spacer plates on the casing. The original impeller is the same as the symmetric impeller in the

Received March 27 2009; accepted for publication April 22 2009: Review conducted by Prof. Zhang Yangjun. (Paper number O09005)
Corresponding author: Hironori Horiguchi, Associate Professor, horiguti@me.es.osaka-u.ac.jp

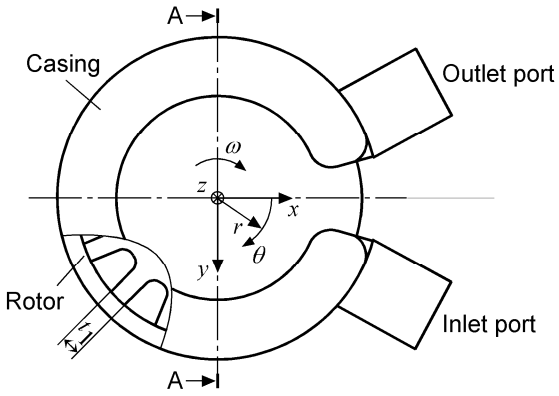

Fig. 1 Schematic of the regenerative pump

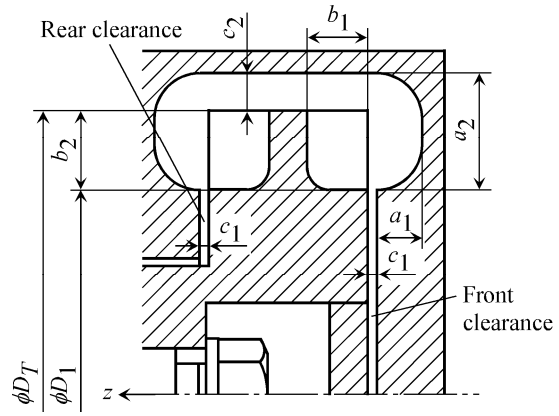

Fig. 2 View of A-A cross section and parameters of the pump

Table 1 Dimensions of the test impeller and casing

Impeller	Number of vanes, Z	16
	Diameter, D_T (mm)	75.0
	Diameter, D_1 (mm)	54.0
	Vane width, t_1 (mm)	5.0
	Channel depth, b_1 (mm)	8.0
	Channel length, b_2 (mm)	10.5
Casing	Channel depth, a_1 (mm)	6.0
	Channel width, a_2 (mm)	15.5
Clearance	Front and rear clearances, c_1 (mm)	1.2, 0.6
	Side clearance, c_2 (mm)	5.0

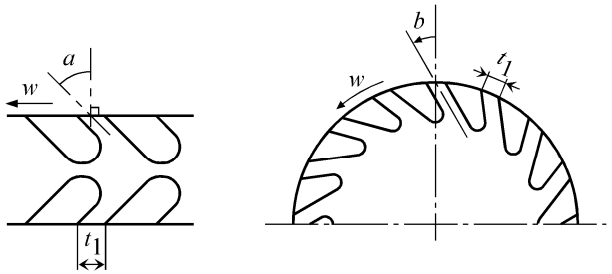

(a) Inlet blade angle (b) Outlet blade angle

Fig. 3 Definition of the inlet and outlet blade angles

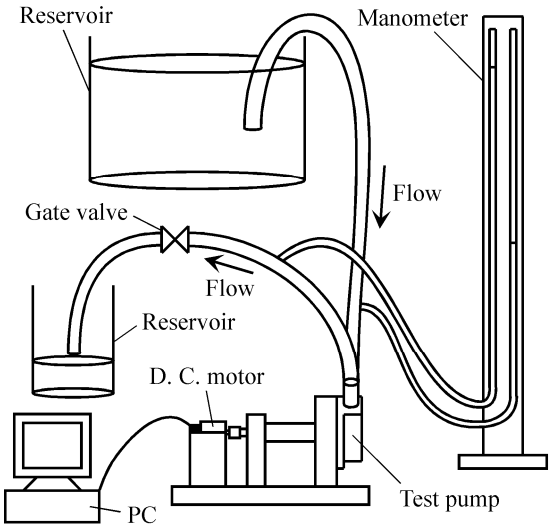

Fig. 4 Experimental setup

study [3]. A lot of researches for general regenerative pumps and fans have been done to clarify the effect of geometries to the performance [4-6]. The values of D_T was determined for high discharge pressure with reference to the study [5]. The geometry of the casing is the same as the casing of the pump with the symmetric impeller in the study [3]. The depth of the vane channel b_1 and the depth of the casing flow path a_1 are 8mm and 6mm, respectively. These values were selected to realize the highest head based on the results of the preliminary tests for micro regenerative pumps [1].

At the beginning, the effects of inlet and outlet blade angles are examined. The definitions of the inlet and outlet blade angles are shown in Figs.3(a) and (b). Figure 3(a) shows the side view of the impeller and the inlet blade angle α is defined as shown in the figure. Figure 3(b) shows the front view and the outlet blade angle β is defined as shown in the figure.

Figure 4 shows the schematic of the experimental setup. The impeller is driven by a blushless servomotor. The rotational speed is 600rpm. The flow rate is adjusted by controlling the downstream valve and estimated from the weight of discharged fluid. The pressure coefficient ψ is estimated from the pressures on the walls of suction and discharge pipes. The pressure taps on the suction and discharge pipes are set about 32 and 40 times of the inner diameter (25mm) of these pipes upstream and downstream from the shaft axis, respectively. The working fluid is water with ambient temperatures (about 25 degrees Celsius). The Reynolds numbers defined by the impeller diameter D_T and the tip speed U_T are about 2.0×10^5. This value is about 10 times of the Reynolds number for the targeted micro pump.

3. Computation

For the flow analysis, a commercial software ANSYS CFX-11.0 was used. Basic equations are the continuity equation and the Reynolds averaged Navier-Stokes equation. SST turbulence model were used.

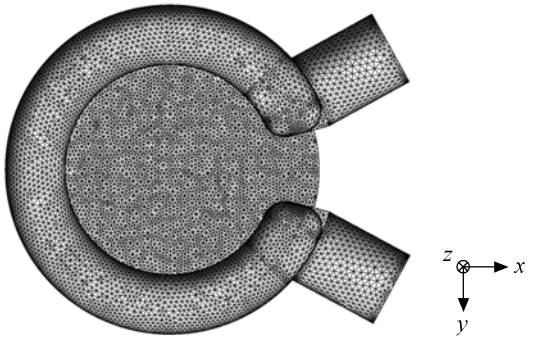

Fig. 5 Computational grid of the casing surface

The computational domain consists of the rotational domain around the impeller, the static domains in the casing, the inlet and outlet pipes. The computational grid on the casing is shown in Fig.5. The geometry of the computational cells is mainly tetrahedral and triangular prism near the wall. The impeller rotates around the *z* axis shown in Fig. 1. The center lines of the inlet and outlet pipes are at $\theta = -28.6\,\mathrm{deg}$ and 28.6deg, respectively. The lengths of the inlet and outlet pipes are about 11.1 and 13.5 times of the casing diameter (only a part is shown in Fig.5). The number of the computational cells for the pump with the clearance $c_1 = 0.6\mathrm{mm}$ is about 200 thousands in the impeller, about 520 thousands in the casing, about 30 thousands in the inlet pipe, about 30 thousands in the outlet pipes, and about 780 thousands in total. The number of the computational cells for the pump with the clearance $c_1 = 1.2\mathrm{mm}$ is about 310 thousands around the impeller, about 740 thousands in the casing, about 60 thousands in the inlet pipe, about 70 thousands in the outlet pipes, and about 1,170 thousands in total.

The static pressure at the inlet, the mass flow rate at the outlet, and a non-slip condition on the wall were given as boundary conditions. Unsteady calculation was performed. The time step is 1/400 of one period of the rotation of the impeller. The results shown in the present study are the results at least after 3 revolutions of the impeller where the fluctuation of the head becomes periodic. Working fluid is water with ambient temperatures.

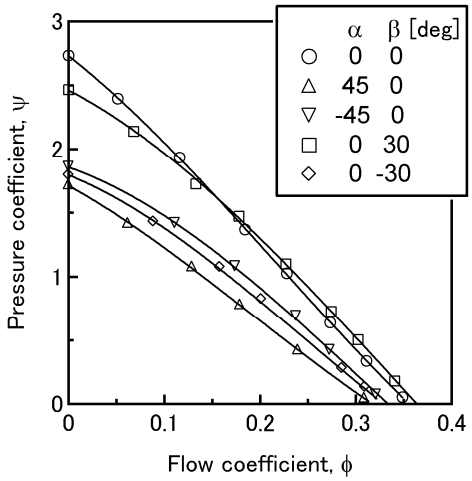

Fig. 6 Experimental performance curve (c_1=1.2mm)

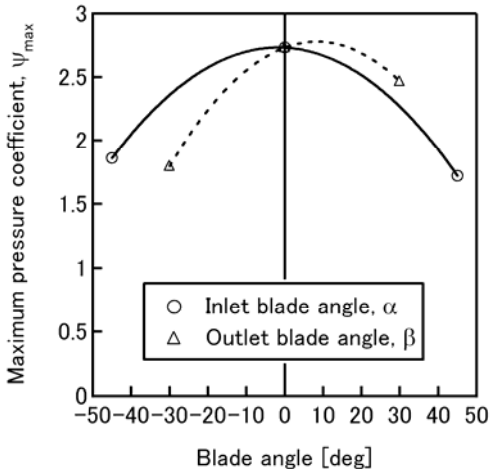

Fig.7 Experimental maximum pressure coefficient (c_1=1.2mm)

4. Results and Discussions

4.1 Effect of the Inlet Blade Angle

In industrial regenerative pumps and fans, the pump head could be increased by optimizing the inlet blade angle [7, 8]. In the present study, experiments for the impellers with the inlet blade angle $\alpha = 0\,\mathrm{deg}$, $45\,\mathrm{deg}$, and $-45\,\mathrm{deg}$ were conducted. The performance curves are shown in Fig. 6. The values of the pressure coefficient ψ in the impellers with $\alpha = \pm 45\,\mathrm{deg}$ are smaller than those in the impellers with $\alpha = 0\,\mathrm{deg}$. The values of ψ at the shutoff flow rate are plotted versus the blade angle in Fig.7. The maximum pressure coefficient ψ_{max} seems to be realized near $\alpha \approx 0\,\mathrm{deg}$.

4.2 Effect of the Outlet Blade Angle

In industrial regenerative pumps and fans, the pump head could be also increased by optimizing the outlet blade angle [7, 9]. The experiments for the impellers with the outlet blade angle $\beta = 0\,\mathrm{deg}$, $30\,\mathrm{deg}$, and $-30\,\mathrm{deg}$ were conducted. The performance curves are shown in Fig. 6. The values of ψ in the impeller with $\beta = 30\,\mathrm{deg}$ are a little larger than those in the impeller with $\beta = 0\,\mathrm{deg}$ in $\phi > 0.15$, but smaller in $\phi < 0.15$. The values of ψ in the impeller with $\beta = -30\,\mathrm{deg}$ are quite smaller than those in the impeller with $\beta = 0\,\mathrm{deg}$. The values of ψ at the shutoff flow rate are plotted versus the blade angle in Fig.7. Maximum pressure coefficient ψ_{max} seems to be realized near $\beta \approx 0\,\mathrm{deg}$.

In our regenerative pump, it was difficult to increase the value of ψ significantly by changing the inlet and outlet blade angles. The reason is not clear. It may be caused by the blockage of the circulating flow between the casing flow path and the vane channel due to the larger blade thickness.

4.3 Effect of the Axial Clearance

In industrial regenerative pumps, the decrease of the axial clearance between the impeller and the casing increases the head [10]. In the present study, the clearance was decreased from c_1=1.2mm of the original to c_1=0.6mm.

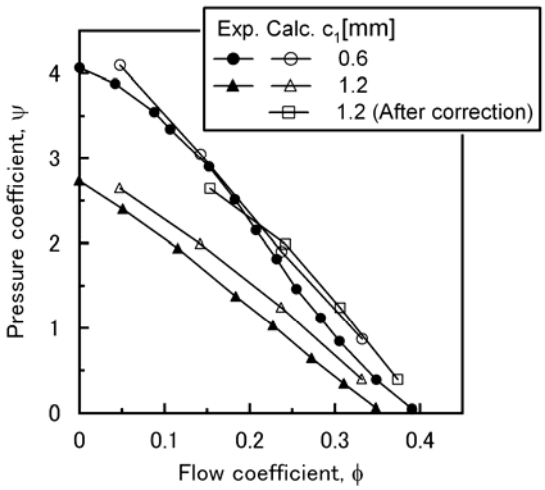

Fig. 8 Experimental and computational performance curves

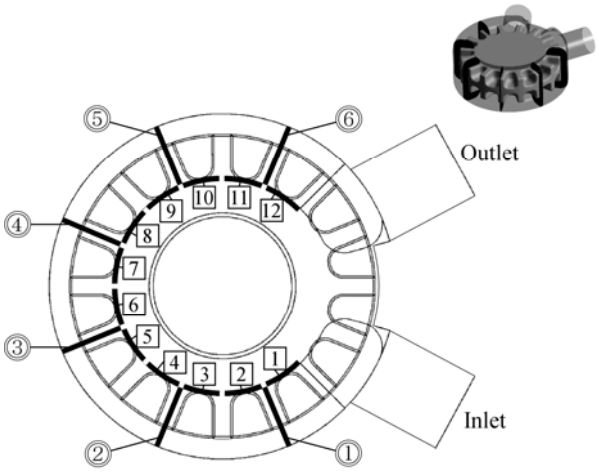

Fig. 9 Control surface for the local flow rate

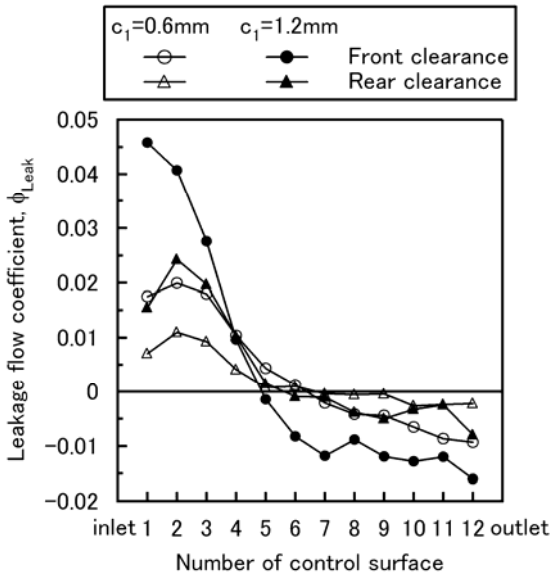

Fig.10 Computational flow rate of the clearance flow at ϕ=0.047

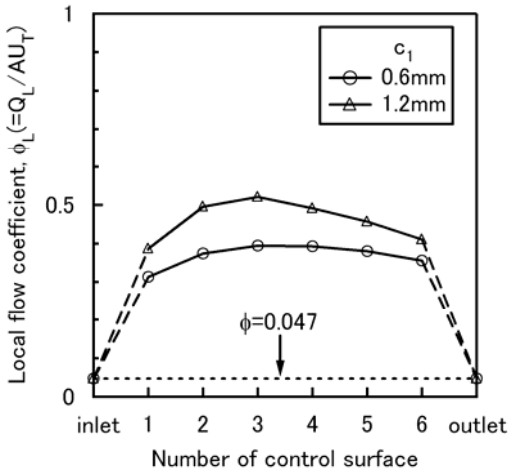

Fig. 11 Computational local flow rate at ϕ=0.047

4.3.1 Performance Curves

The performance curves of the pumps with $\alpha = \beta = 0\,\mathrm{deg}$ and c_1=0.6, 1.2mm are shown in Fig.8. Both experimental and computational results are plotted. It is found that the value of ψ was drastically increased by the decrease of the clearance c_1 from 1.2mm to 0.6mm. The value of ψ in the case of c_1=0.6mm is about 1.4times larger than that in the case of c_1=1.2mm at the shutoff flow rate.

Although the agreement is only qualitative, the computational results can simulate the effect of the clearance.

4.3.2 Flow Rates Through the Clearance and the Casing Flow Path

In order to clarify the cause of the increase of ψ due to the decrease of c_1, the internal flow was examined based on the computational results.

The lines indicated by the numbers 1-12 in squares in Fig.9 show the control surfaces at the outer edge of the front clearance shown in Fig.2 for estimating the flow rate through the front clearance. The axial width of the control surfaces is the same as the clearance c_1. The control surfaces are also set up at the outer edge of the rear clearance shown in Fig.2. Figure 10 shows the flow rate $\phi_{Leak}\ (=Q_{Leak}/(AU_T))$ of the fluid which goes through the control surfaces at the flow rate ϕ=0.047. The flow rate of radially-outward flow is positive. In comparison with the net flow rate ϕ=0.047, the leakage flow rate ϕ_{Leak} is significant in both cases of c_1=0.6mm and 1.2mm. The flow rate ϕ_{Leak} in the case of c_1=0.6mm is about a half of that in the case of c_1=1.2mm.

The lines indicated by the doubly encircled numbers 1-6 in Fig.9 show the control surfaces in the casing (it does not include the part between vanes). The figures in the upper right of Fig.9 also show the control surfaces. Figure 11 shows the local flow rate $\phi_L(=Q_L/(AU_T)=\overline{v}_\theta/U_T)$ of the fluid which goes through the control surfaces. The value of ϕ_L of the pump with c_1=0.6mm is smaller than that of the pump with c_1=1.2mm. The local flow rate ϕ_L of both pumps are quite larger than the net flow rate ϕ=0.047.

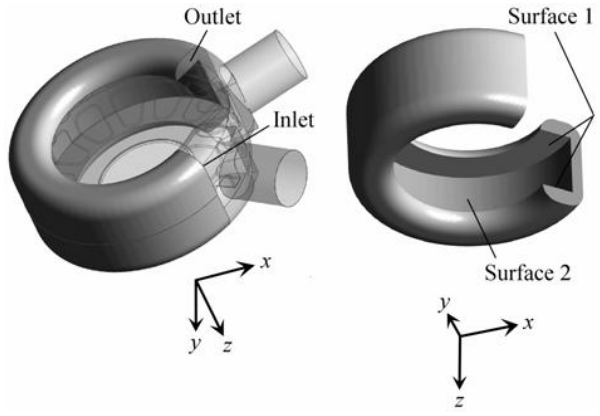

Fig.12 Control volume and surfaces for the estimation of angular momentum

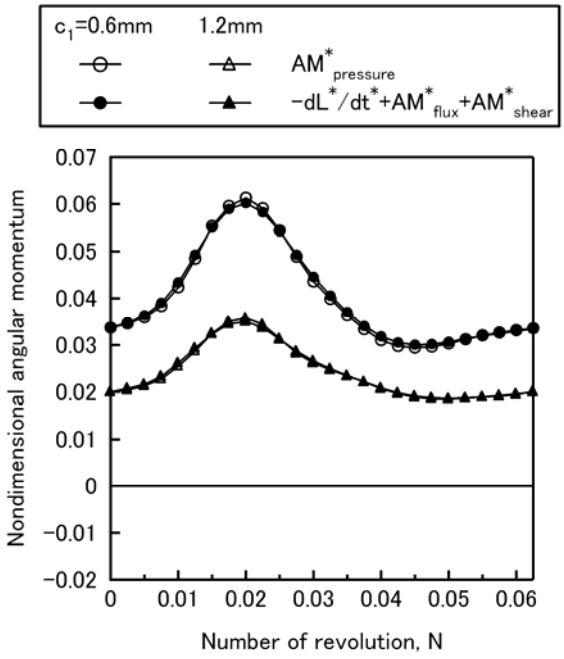

Fig. 13 Conservation of angular momentum at ϕ=0.047

In Fig. 11, the averaged local flow rates $\bar{\phi}_L$ of the fluid which goes through the control surfaces with numbers 1-6 are 0.37 in the case of c_1 =0.6mm and 0.46 in the case of c_1 =1.2mm, respectively. The averaged local flow rates $\bar{\phi}_L$ were calculated for the cases with c_1 =0.6mm and 1.2mm. Then, the difference of these values were added to the flow rate of the performance curve of c_1 =1.2mm. The performance curve after correction is also shown in Fig.8. The corrected performance curve are similar to the performance curve of c_1 =0.6mm. This suggests that the increase of the pressure coefficient were caused by the decrease of the flow rate through the casing due to the decrease of the leakage flow.

4.3.3 Angular Momentum

The angular momentum in the casing was investigated to clarify the relation between the leakage flow and the pressure coefficient. Figure 12 shows a control volume. The control volumes are set in the casing flow path excluding the inlet and outlet regions ($-45\,\mathrm{deg} < \theta < 45\,\mathrm{deg}$). Surface 1 of the control volume are located at the axial distance of c_1 from the side of the impeller vane. Surface 2 of the control volume is located at a radial distance of 1.0mm from the tip of the impeller.

We consider the conservation of the angular momentum around the axis of the impeller using the cylindrical coordinate system shown in Fig.1. Since the temporal change of the angular momentum due to the impeller vane passage is not negligible, we use the unsteady conservation law of the angular momentum.

$$AM^*_{pressure} = -\frac{dL^*}{dt^*} + AM^*_{flux} + AM^*_{shear} \qquad (1)$$

where

$$AM^*_{pressure} = \left(\sum_i r_i \cdot \Delta a_{outlet,i} \cdot p_{outlet,i} - \sum_i r_i \cdot \Delta a_{inlet,i} \cdot p_{inlet,i} \right) / \left(\rho U_T^2 D_T^3 \right)$$

$$L^* = \rho \sum_i \Delta V_i \cdot r_i \cdot v_{\theta,i} / \left(\rho U_T D_T^4 \right)$$

$$AM^*_{flux} = \left(\sum_i \Delta \dot{m}_{in,i} \cdot r_i \cdot v_{\theta,i} - \sum_i \Delta \dot{m}_{out,i} \cdot r_i \cdot v_{\theta,i} \right) / \left(\rho U_T^2 D_T^3 \right)$$

$$AM^*_{shear} = T / \left(\rho U_T^2 D_T^3 \right)$$

$$t^* = t / \left(D_T / U_T \right)$$

$AM^*_{pressure}$ is the moment of the pressure forces at the inlet and outlet boundary. L^* is the angular momentum in the control volume, AM^*_{flux} is the angular momentum of the fluid entering the control volume, AM^*_{shear} is the moment due to the shear force on the surface of the control volume, and t^* is the nondimensional time.

4.3.4 Effect of the Clearance on Angular Momentum

Figure 13 shows the value of $AM^*_{pressure}$ on the left hand side of Eq.(1) and the value of $-dL^*/dt^* + AM^*_{flux} + AM^*_{shear}$ on the right hand side of Eq.(1). Since the number of vanes is 16, the angular momentum fluctuates with one sixteenth of the rotational period. Therefore, the results in one sixteenth periods are shown. At the number of revolution of N=0, the center lines of vanes are at θ=45deg and -45deg, i.e., at the inlet and outlet surfaces of the control volume, respectively. The values of $AM^*_{pressure}$ and $-dL^*/dt^* + AM^*_{flux} + AM^*_{shear}$ are nearly equal and the conservation law are satisfied fairly well in both cases of c_1 =0.6mm and 1.2mm.

Figure 14 shows the values of $-dL^*/dt^*$, AM^*_{flux} and AM^*_{shear}. It is found that the temporal changes of $AM^*_{pressure}$ are mainly due to $-dL^*/dt^*$. As the value of AM^*_{flux} is larger than the average of $-dL^*/dt^*$ and the value of AM^*_{shear}, we can say

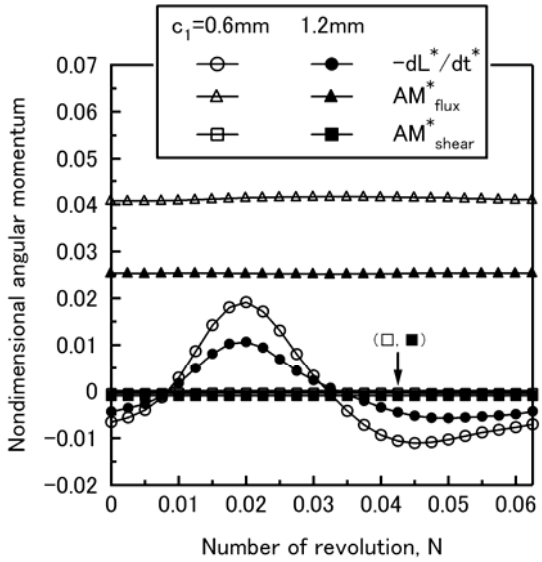

Fig. 14 Angular momentum at ϕ=0.047

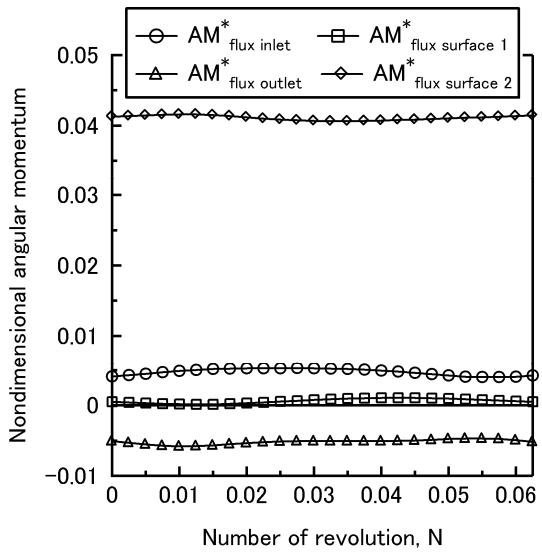

Fig.15 Angular momentums supplied by fluxes from Inlet, Outlet, Surface 1 and Surface 2 of the control volume in the pump with c_1=0.6mm at ϕ=0.047

that the pressure rise of the pump is mainly caused by AM^*_{flux}.

The averages of $-dL^*/dt^*$ and the values of AM^*_{shear} are nearly equal in both cases of c_1=0.6mm and 1.2mm. The value of AM^*_{flux} of the pump with c_1=0.6mm is about 1.6 times as large as that of the pump with c_1=1.2mm. It is found that the influence of the difference of c_1 largely appears in the value of AM^*_{flux}.

4.3.5 Angular Momentum of the Flow Entering the Control Volume

Figures 15 and 16 show the values of the angular momentum which enters the control volume in the case of c_1=0.6mm and 1.2mm, respectively. $AM^*_{flux\ inlet}$, $AM^*_{flux\ outlet}$, $AM^*_{flux\ surface1}$ and $AM^*_{flux\ surface2}$ are the angular momenta which flow into the control volume through the inlet and outlet surfaces, and the surfaces near the impeller (Surface 1 and 2) shown in Fig.12. Absolute values of $AM^*_{flux\ inlet}$ and $AM^*_{flux\ outlet}$ are similar and their signs are opposite. Therefore, $AM^*_{flux\ inlet}$ and $AM^*_{flux\ outlet}$ do not contribute to the pressure rise. $AM^*_{flux\ surface2}$ of both pumps with c_1=0.6mm and 1.2mm largely contribute to the pressure rise.

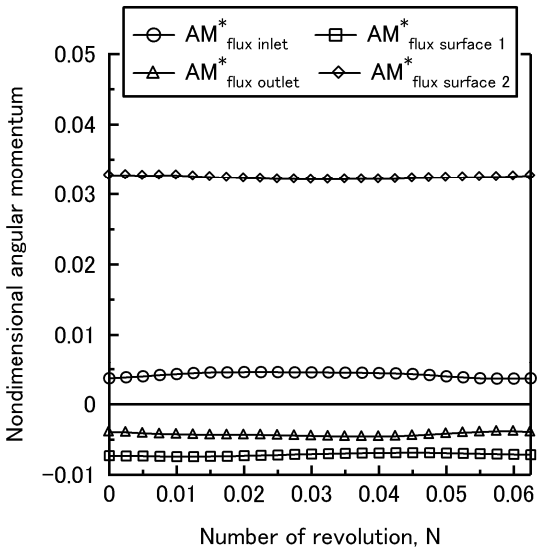

Fig. 16 The same as Fig.15, for c_1=1.2mm

The values of $AM^*_{flux\ surface1}$ and $AM^*_{flux\ surface2}$ with c_1=0.6mm are larger than those with c_1=1.2mm. To clarify the cause of that, a flow rate $\phi_c (= Q_c/(AU_T))$ of the fluid which flows into/out from the control volume through Surface 1 and 2 and its averaged circumferential velocity $\overline{v}_\theta / U_T$ were examined. The results at a number of the revolution of $N = 0$ are shown in Table 2. The right column in Table 2 shows the ratio of $\overline{v}_\theta / U_T$ of outflow to that of inflow. Although the difference of ϕ_c of the inflow and outflow from Surface 1 and 2 exists, the continuity equation is satisfied if we consider the inflow and outflow from the surfaces of Inlet and Outlet shown in Fig.12.

From these results, it was found that the higher pressure rise was realized in the pump with c_1=0.6mm because the difference of the angular momenta which flow into/out from the control volume is larger than that of the pump with c_1=1.2mm due to the larger deceleration ratio which is caused by the decrease of the local flow rate ϕ_L.

Figure 17 shows the meridional velocity vectors and velocity distributions of v_θ / U_T on the meridian plane at θ=191.25deg at a number of the revolution of N=0. Figures 17(a) and (b) show the results for the pumps with c_1=0.6mm and 1.2mm, respectively. The values of v_θ / U_T of the fluid which flows into the control volume through Surface 2 is smaller in both pumps with c_1=0.6mm and 1.2mm. The values of v_θ / U_T of the fluid which flows out from the control volume through Surface 1 in the pump with c_1=0.6mm is quite smaller than those of the pump with c_1=1.2mm, caused by smaller local flow rate. In summary, the increase of pressure rise associated with the decrease of the clearance c_1 is caused by the increase of the angular momentum supplied into the casing flow path due to the decrease of the circumferential velocity entering the impeller, which is caused by the decrease of the leakage flow and hence local flow rate.

5. Conclusions

The effect of the inlet and outlet blade angles, and the axial clearance between the impeller and casing on the pressure performance of micro regenerative pump was investigated in experiments and computations. The following results were obtained.

(1) In the regenerative pump with larger blade thickness and larger axial clearance between the impeller and the casing in the present study, the pressure coefficient does not change largely by changing the inlet and outlet blade angles from 0deg.
(2) The pressure coefficient can be increased by decreasing the axial clearance between the impeller and the casing.
(3) Due to the decrease of the axial clearance, the leakage flow rate in the clearance and the local flow rate through the casing flow path decrease.
(4) The increase of the pressure coefficient due to the decrease of the axial clearance is caused by the increase of the angular momentum supplied into the casing flow path due to the decrease of the circumferential velocity entering the impeller.

Acknowledgement

This study was financially supported by the Comprehensive Support Programs for Creation of Regional Innovation which is provided by the Japan Science and Technology Agency (JST).

Nomenclature

a_1	Depth of the casing flow path [m]	Q_L	Local volume flow rate through the casing flow path [m^3/s]
a_2	Radial width of the casing flow path [m]		
Δa	Minute area on the surface of the control volume [m^2]	Q_{Leak}	Volume flow rate of the leakage flow through the clearance [m^3/s]
A	Area in the meridional plane (vane section not included) of the casing flow path [m^2]	r	Radial coordinate
		t	Time [s]
AM^*_{flux}	Angular momentum of the fluid which flows into/out from the control volume, Eq.(1)	t_1	Thickness of vane [m]
		t^*	Nondimensional time, Eq.(1)
		T	Torque [N·m]
$AM^*_{flux\ inlet}$	Angular momentum of the fluid which flows into the control volume through the inlet surface, Eq.(1)	U_T	Tip velocity of the impeller [m/s]
		v_θ	Circumferential velocity [m/s]
		$\overline{v}_\theta$	Average circumferential velocity [m/s]
$AM^*_{flux\ outlet}$	Angular momentum of the fluid which flows into the control volume through the outlet surface, Eq.(1)	z	Axial coordinate
		α	Inlet blade angle [deg]
		β	Outlet blade angle [deg]
$AM^*_{flux\ surface1}$, $AM^*_{flux\ surface2}$	Angular momentum of the fluid which flows into/out from the control surfaces near the impeller	$\Delta\dot{m}_{in}$	Mass flow rate of the fluid which flows into the minute area on the control volume [kg/s]
		$\Delta\dot{m}_{out}$	Mass flow rate of the fluid which flows out from the minute area on the control volume [kg/s]
$AM^*_{pressure}$	Moment generated by a pressure, Eq.(1)		
AM^*_{shear}	Moment generated by a shear force, Eq.(1)		
b_1	Depth of the vane channel [m]	ΔV	Minute volume of the control volume [m^3]
b_2	Radial width of the vane channel [m]	ϕ	Flow coefficient $= Q/(AU_T)$
c_1	Axial clearance between the impeller and the casing [m]	ϕ_c	Local flow coefficient $= Q_c/(AU_T)$
		ϕ_L	Local flow coefficient in the casing flow path $= Q_L/(AU_T)$
c_2	Radial clearance between the impeller and the casing [m]	ϕ_{Leak}	Local flow coefficient of the leakage flow $= Q_{Leak}/(AU_T)$
D_1	Inner diameter of the casing flow path [m]		
D_T	Diameter of the impeller [m]	θ	Circumferential coordinate
g	Gravity [m/s^2]	ρ	Density [kg/m^3]
L^*	Nondimensional angular momentum,Eq.(1)	ω	Angular velocity of the impeller [rad/s]
N	Number of the revolution of the impeller	ψ	Pressure coefficient $= (p_2 - p_1)/(\rho U_T^2/2)$
p	Pressure [Pa]		
p_1	Pressure at the inlet [Pa]	Subscript	
p_2	Pressure at the outlet [Pa]	i	Number of the minute elements on the control volume
Q	Volume flow rate [m^3/s]		
Q_c	Volume flow rate of the fluid which flows into/out from the control volume through the control surfaces near the impeller [m^3/s]	*inlet*	Inlet surface of the control volume
		outlet	Outlet surface of the control volume

References

[1]Yumiba, D., 2005, “Prototyping of Micro Pump and the Reynolds Number Effect on the Performance of Micro Regenerative Pump,” Master Thesis, Osaka University, in Japanese.

[2]Horiguchi, H., Yumiba, D., Tsujimoto, Y., Sakagami, M., and Tanaka, S., 2008, “Reynolds Number Effect on Regenerative Pump Performance in Low Reynolds Number Range,” International Journal of Fluid Machinery and Systems, Vol. 1, No. 1, pp. 101-108.
[3]Horiguchi, H., Matsumoto, S., Tsujimoto, Y., Sakagami, M., and Tanaka, S., 2009, “Effect of Internal Flow in Symmetric and Asymmetric Micro Regenerative Pump Impellers on Their Pressure Performance,” International Journal of Fluid Machinery and Systems, Vol. 2, No. 1, pp. 72-79.
[4]Iversen, H. W., 1955, “Performance of the Periphery Pump,” Transactions of the ASME, Vol. 77, pp. 19-22.
[5]Shimosaka, M. and Yamazaki, S., 1960, “Research on the Characteristics of Regenerative Pump (1st Report, Influences of Flow Channel and Impeller),” Bulletin of the JSME, Vol. 3, No. 10, pp. 185-190.
[6]Inaba, T., Hayashi, M, and Murata, S., 1981, “A Study on a Vortex Blower (1st Report, Effect of the Shape of Impeller and Modification of the Inlet of Blower),” Bulletin of the JSME, Vol. 24, No. 192, pp. 973-979.
[7]Inaba, T., Hayashi, M., Murata, S., and Kawatani, Y., 1982, “A Study on a Vortex Blower (2nd Report, Effect of the Blade Angles and a Theoretical Analysis of the Performance),” Bulletin of the JSME, Vol. 25, No. 200, pp. 157-164.
[8]Hubel, M., Blattel, B., and Strohl, W., 1995, “Investigation of Fluid Mechanics of the Regenerative Pump Used in Gasoline Injection Systems,” SAE TECHNICAL PAPER SERIES, International Congress and Exposition, Detroit, Michigan, No. 950077, pp. 131-139.
[9]Yamazaki, S. and Tomita, Y., 1971, “Researches on the Performance of the Regenerative Pump with Non-Radial Vanes (1st Report, Performance and Inner Flow),” Bulletin of the JSME, Vol. 14, No. 77, pp. 1178-1186.
[10]Yamazaki, S., Tomita, Y., and Sasahara, T., 1972, “Researches on the Performance of the Regenerative Pump with Non-Radial Vanes (2nd Report, Effects of the Pump Elements),” Bulletin of the JSME, Vol. 15, No. 81, pp. 337-343.